


Article

Oxidation of Toluene by Ozone over Surface-Modified γ -Al₂O₃: Effect of Ag Addition

Kandukuri Bhargavi¹, Debjyoti Ray¹, Piu Chawdhury¹, Sairam Malladi², Thatikonda Shashidhar³ 
and Challapalli Subrahmanyam^{1,*}

¹ Department of Chemistry, Indian Institute of Technology Hyderabad, Hyderabad 502 285, India; cy19resch01001@iith.ac.in (K.B.); cy15resch01004@iith.ac.in (D.R.); cy16resch11006@iith.ac.in (P.C.)

² Department of Materials Science and Metallurgical Engineering, Indian Institute of Technology Hyderabad, Hyderabad 502 285, India; srkm@msme.iith.ac.in

³ Department of Civil Engineering, Indian Institute of Technology Hyderabad, Hyderabad 502 285, India; shashidhar@ce.iith.ac.in

* Correspondence: csubbu@iith.ac.in

Abstract: In this study, the ability of ozone to oxidise toluene present in low levels into CO and CO₂ was studied. The catalytic ozonation of toluene was carried out in a micro-fixed bed reactor. The oxidation was done in two steps: toluene adsorption on the catalyst followed by sequential ozone desorption. Toluene breakdown by ozone at low temperature and atmospheric pressure was achieved using γ -Al₂O₃ supported transition metal oxides impregnated with a reduced noble metal. The catalyst Ag-CoO_x/ γ -Al₂O₃ efficiently oxidised and transformed toluene into products (52.4% CO_x yield). This catalyst has a high surface area, more acidic sites, and lattice oxygens for better toluene oxidation. The addition of Ag to the CoO_x/ γ -Al₂O₃ catalyst surface improved toluene adsorption on the catalyst surface, resulting in improved product yield, selectivity, and carbon balance.



Citation: Bhargavi, K.; Ray, D.; Chawdhury, P.; Malladi, S.; Shashidhar, T.; Subrahmanyam, C. Oxidation of Toluene by Ozone over Surface-Modified γ -Al₂O₃: Effect of Ag Addition. *Catalysts* **2022**, *12*, 421. <https://doi.org/10.3390/catal12040421>

Academic Editors: Junling Lu and Qiang Fu

Received: 26 February 2022

Accepted: 6 April 2022

Published: 8 April 2022

Publisher's Note: MDPI stays neutral with regard to jurisdictional claims in published maps and institutional affiliations.



Copyright: © 2022 by the authors. Licensee MDPI, Basel, Switzerland. This article is an open access article distributed under the terms and conditions of the Creative Commons Attribution (CC BY) license (<https://creativecommons.org/licenses/by/4.0/>).

Keywords: VOC; transition metal oxides; catalytic ozonation

1. Introduction

The volatile organic compounds from paints, furnishings and sprays are the leading causes of indoor air pollutants. Industrial and vehicular exhausts and other human activities lead to outdoor air pollution [1]. Nowadays, people spend a long time indoors for work and family. Hence, indoor air purification technologies are gaining importance [2]. Several methods, such as sorption techniques [3], biofiltration [4], photocatalytic oxidation [5] and non-thermal plasma [6–8], are used to remove indoor air pollutants [9–11]. Thermal incineration is helpful in many applications, but heterogeneous catalysis can improve efficiency [12,13]. Catalytic oxidation drastically reduces the reaction temperature of VOCs from ~1000 °C in thermal oxidation to around ~250 °C [14].

Catalytic oxidation technology is generally used for industrial applications due to its wide adaptability to a significant number of VOCs. Liu and co-workers obtained a conversion of ~94% benzene using birnessite-type MnO₂ synthesised via the green synthesis method [15]. The ability of MnO_x/TiO₂ composite nanofibers for the complete oxidation of acetone was demonstrated by Zhu et al. [16]. A few groups, such as Shi et al. [17] and Wang et al. [18], have studied the role of different morphologies of MnO_x in the catalytic combustion of toluene. Catalytic oxidation is highly exothermic and works for high input VOC concentrations. However, when the reactant concentration is low, it is not economical to carry out these reactions. Combining catalytic oxidation technology with proper combustion technology will reduce the reaction temperature and completely degrade VOCs [14]. In this regard, catalytic oxidation using ozone is an alternative and effective method to destroy VOCs. There are numerous studies on the oxidation of various VOCs with ozone. Zhoa et al. studied the effect of water vapour on catalytic ozonation of formaldehyde over MnO_x. They demonstrated that humid air reduces the accumulation of

carbonate species over the catalyst [19]. Lin and co-workers studied the degradation of mixed Cl-VOCs by catalytic ozonation over MnO_x impregnated on different supports [20].

Many studies have also focused on using either noble metals or transition metal oxides unsupported or supported on materials with a high specific surface area such as Al_2O_3 , TiO_2 , SiO_2 , etc. Tian and co-workers studied the degradation of gaseous methanol at normal temperature using Pt/ FeO_x [21]. He et al. used wet scrubbing along with catalytic ozonation for the first time to eliminate CH_3SH using Ag/ MnO_2 [22]. Though noble metals are efficient for VOC degradation, their high cost limits their usage. Transition metal oxides such as Cu, Fe, Co, Mn, and Ni have been widely studied for VOC degradation under ozone flow. Furthermore, the type of material used as support plays a crucial part in aiding the catalyst activity. Al_2O_3 is the most used support material for its large surface area, moderate chemical activity, and low cost [23,24]. Hence, modifying the support system with different metal oxides (mono or bimetallic) may greatly enrich the catalytic activity. Even though numerous studies have focused on the role of Mn oxides in VOC degradation, there are few reports on Co-based oxides.

The current work looks at transition metal-based heterogeneous catalysts ($\gamma\text{-Al}_2\text{O}_3$ supported Mn, Co, and Ag catalysts) in the ozone-assisted toluene degradation process. Furthermore, the oxidation products, CO and CO_2 , are quantified, and the limitations of catalytic ozonation of toluene are analysed. The plausible reasons for the improved activity of the catalytic systems are evaluated.

2. Results and Discussion

2.1. XRD

Figure 1 depicts the synthesised catalysts' X-ray diffraction (XRD) patterns. All the catalysts display three major diffraction peaks at $2\theta = 37.5^\circ$, 46.2° and 66.8° , corresponding to (311), (400) and (440) planes of crystalline $\gamma\text{-Al}_2\text{O}_3$ (Joint Committee on Powder Diffraction Standards (JCPDS)-290063), respectively. Peaks with 2θ at 37.3° , 42.9° and 56.9° corresponding to (110), (101), and (102) planes, respectively, can be assigned to MnO_2 in $\text{MnO}_x/\gamma\text{-Al}_2\text{O}_3$ and Ag- $\text{MnO}_x/\gamma\text{-Al}_2\text{O}_3$ (JCPDS 72-1982). Low intense peaks observed at $2\theta = 36.8^\circ$ and 65.2° (merged with $\gamma\text{-Al}_2\text{O}_3$ peak) match the (311) and (440) planes of Co_3O_4 in $\text{CoO}_x/\gamma\text{-Al}_2\text{O}_3$ and Ag- $\text{CoO}_x/\gamma\text{-Al}_2\text{O}_3$ (JCPDS 78-1970), suggesting that Co is highly dispersed on the support. XRD patterns of Ag in Ag/ $\gamma\text{-Al}_2\text{O}_3$, Ag- $\text{MnO}_x/\gamma\text{-Al}_2\text{O}_3$ and Ag- $\text{CoO}_x/\gamma\text{-Al}_2\text{O}_3$ were not distinct amid the other metal oxide peaks, possibly due to the high distribution of Ag particles on the support.

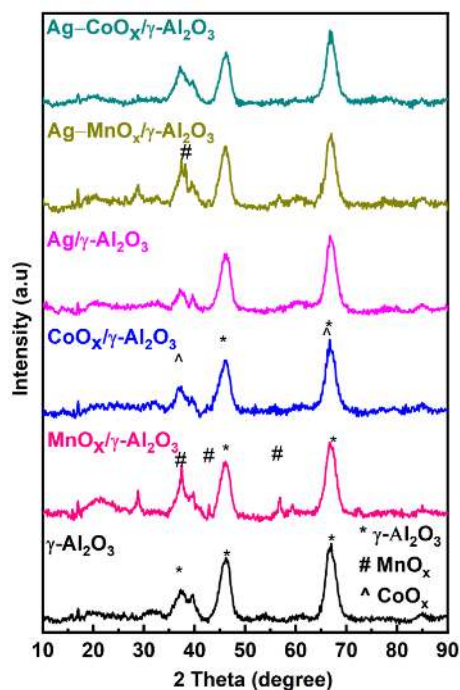


Figure 1. XRD patterns of the bare and metal oxide modified $\gamma\text{-Al}_2\text{O}_3$; * $\gamma\text{-Al}_2\text{O}_3$, # MnO_x , ^ CoO_x .

2.2. Physisorption

Brunauer-Emmett-Teller (BET) surface area, average pore diameter and total pore volume of the synthesised catalysts are summarised in Table 1. The induction of Mn and Co on γ -Al₂O₃ leads to blocked pore diameter, and consequently, the BET surface area is less than bare γ -Al₂O₃. The introduction of silver on γ -Al₂O₃ and the other two catalysts (MnO_x/ γ -Al₂O₃ and CoO_x/ γ -Al₂O₃) positively increased the surface area. Figure 2a and b show the N₂ adsorption and desorption isotherms and the pore size distribution curves of the fresh catalysts. All catalysts exhibited Type-V isotherm with H3 type hysteresis loop in the range of 0.4 to 0.95 P/P₀, indicating the catalysts' mesoporous nature.

Table 1. Physio-chemical properties of the catalysts.

Catalysts	Surface Area (m ² /g)	Total Pore Volume (cc/g)	Average Pore Diameter (nm)	O _{latt} /O _{surf}
γ -Al ₂ O ₃	293	0.83	11.36	0.85
MnO _x / γ -Al ₂ O ₃	256	0.7	10.94	0
CoO _x / γ -Al ₂ O ₃	253	0.72	11.34	0
Ag/ γ -Al ₂ O ₃	272	0.78	11.44	0
Ag-MnO _x / γ -Al ₂ O ₃	265	0.77	11.62	0.80
Ag-CoO _x / γ -Al ₂ O ₃	267	0.76	11.35	1.1

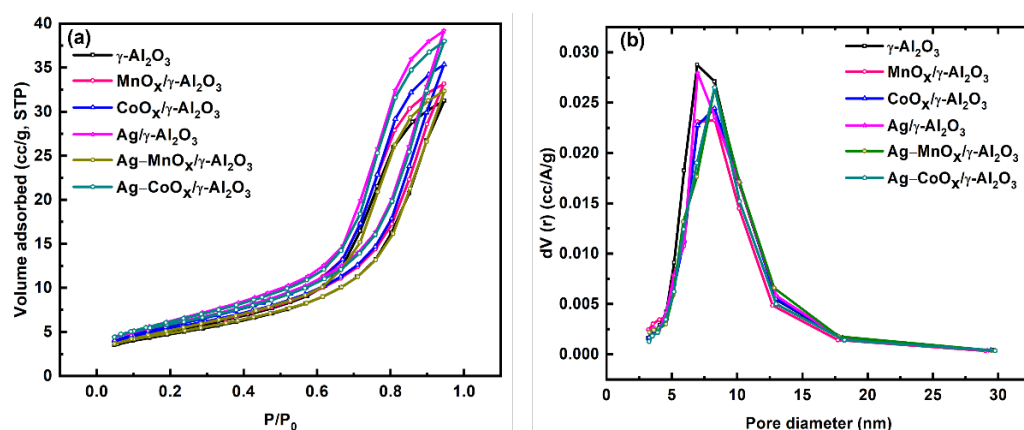


Figure 2. (a) N₂ adsorption-desorption isotherms. (b) Pore size distribution of fresh catalysts.

2.3. CO₂ TPD Analysis and NH₃ TPD Analysis

CO₂ TPD (Temperature programmed desorption) was conducted to account for the basic sites in the catalysts. Figure 3a depicts the corresponding TPD profiles of the as-synthesised catalysts. Except for γ -alumina, all other catalysts showed three desorption peaks in the temperature range of 110–300 °C, 350–475 °C and 500–700 °C, related to weak, moderate, and strong basic sites, respectively. From Table 2, MnO_x/ γ -Al₂O₃ and γ -Al₂O₃ had similar basic strengths. The addition of Ag reduced the number of basic sites. For evaluating acidic sites in the catalysts, NH₃ TPD was done, and the TPD profiles of the catalysts are presented in Figure 3b. Broad peaks were observed for all the catalysts in the temperature range of 110–450 °C, while a comparatively sharp peak was observed in the higher temperature range of 500–750 °C, suggesting the presence of strong acidic sites in this region. The overall concentration of acidic sites increased with Ag addition to Mn and Co catalysts. This could be due to the acidic sites originating from the dispersion and interaction of Ag with Mn and Co [25]. Additionally, the ratio of acidic sites to basic sites (S_a/S_b) was determined to account for the catalysts' activity. The order is as follows: Ag-CoO_x/ γ -Al₂O₃ > CoO_x/ γ -Al₂O₃ > Ag-MnO_x/ γ -Al₂O₃ > Ag/ γ -Al₂O₃ > γ -Al₂O₃ > MnO_x/ γ -Al₂O₃. A comparison of the acidic and basic sites in various temperature ranges is shown in Table 2. The results indicate that the acid sites are more abundant in Ag-CoO_x/ γ -Al₂O₃, which is beneficial for the toluene adsorption, activation, and oxidation.

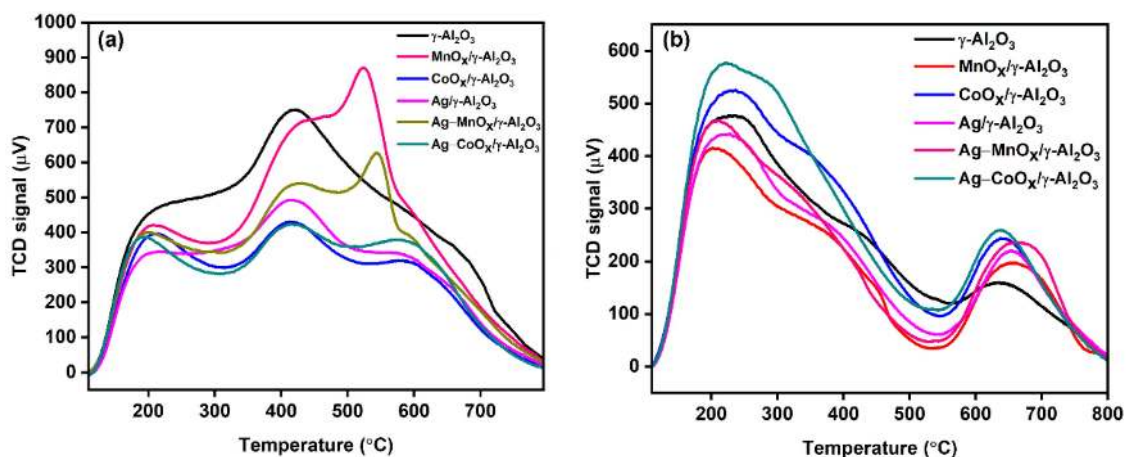


Figure 3. (a) CO₂-TPD profiles, (b) NH₃-TPD profiles of the fresh catalysts.

Table 2. A comparison table of acidic and basic sites of freshly prepared catalysts.

Catalysts	Acidic Sites (mmol/g)				Basic Sites (mmol/g)				S _a /S _b
	Weak	Medium	Strong	Total (S _a)	Weak	Medium	Strong	Total (S _b)	
γ-Al ₂ O ₃	0.209	0.077	0.064	0.35	0.183	0.346	0.182	0.711	0.492
MnO _x /γ-Al ₂ O ₃	0.122	0.098	0.072	0.292	0.128	0.256	0.32	0.704	0.414
CoO _x /γ-Al ₂ O ₃	0.176	0.142	0.087	0.405	0.125	0.186	0.141	0.452	0.896
Ag/γ-Al ₂ O ₃	0.045	0.105	0.08	0.23	0.083	0.24	0.121	0.444	0.518
Ag-MnO _x /γ-Al ₂ O ₃	0.127	0.115	0.087	0.329	0.122	0.174	0.163	0.459	0.716
Ag-CoO _x /γ-Al ₂ O ₃	0.156	0.179	0.102	0.437	0.109	0.279	0.087	0.475	0.920

2.4. XPS

X-ray photoelectron spectroscopy (XPS) analysis confirmed Mn, Co, and Ag's elemental state on the γ-Al₂O₃ surface. Figure 4 illustrates all the characteristic spectra of the synthesised catalysts. The XPS spectra of Mn2p for all the catalysts are shown in Figure 4a. Mn³⁺ and Mn⁴⁺ are the dominant oxidation states found in the prepared catalysts. The binding energies were divided between Mn³⁺ and Mn⁴⁺. The peaks at binding energies 640.5 eV and 640.09 eV corresponding to Mn2p_{3/2} could be assigned to Mn³⁺, and peaks at 644.3 eV corresponding to Mn2p_{3/2} could be designated Mn⁴⁺ [26,27]. Co2p spectrum for the synthesised catalysts can be disintegrated into two distinctive peaks (Figure 4b). Two spin doublets ascribed to CoO_x between 780–781.5 eV and 796–796.6 eV are related to Co2p_{3/2} and Co2p_{1/2}. The spin-orbit doublet of Co2p_{3/2} between 780–781 eV can be deconvoluted into Co³⁺ and Co²⁺. Satellite peaks near the spin-orbit doublets imply cobalt oxides [28]. The two peaks in the Ag-loaded catalysts depicted in Figure 4c can be assigned to Ag3d_{5/2} at 368.0 eV and Ag3d_{3/2} at 374.0 eV. A slight shift of the binding energies from 368 eV to 367.2 eV on the Ag-MnO_x/γ-Al₂O₃ catalyst indicates an oxidised form of silver species [29]. The O1s spectra are represented in Figure 4d around 531 eV. Peak deconvolution suggested two types of oxygen molecules. The peak at the lower binding energy of 529.6 eV relates to lattice oxygen (O_{latt}). In comparison, the peak near the binding energy of 530.7–531 eV corresponds to the surface-adsorbed oxygen (O_{surf}) [29]. The ratios of O_{latt} to O_{surf} for the synthesised catalysts are listed in Table 1. Al2p showed a single peak near 74.1 eV for γ-Al₂O₃ modified by metal oxides. Bare γ-Al₂O₃ displayed a peak at 73.3 eV (Figure 4e) [30].

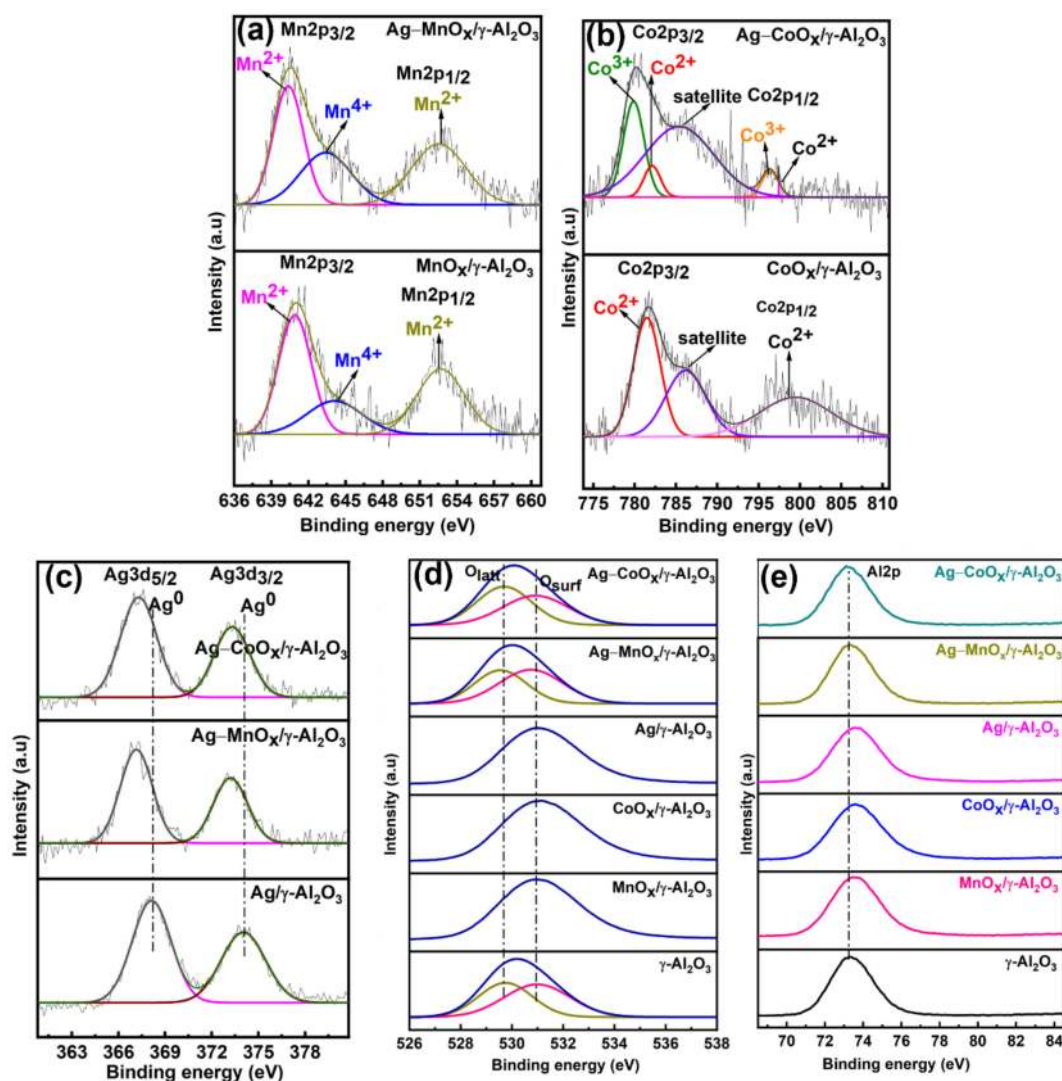


Figure 4. XPS spectra of the prepared catalysts (a) Mn2p, (b) Co2p, (c) Ag3d, (d) O1s and (e) Al2p.

2.5. Catalytic Activity

For adsorption and catalytic ozonation, the catalysts must possess higher adsorption capacities to make them economically viable on an industrial scale. According to a previous study, lower metal loading promotes toluene oxidation up to 80 °C [29]. As a result, the metal oxide loading in the current investigation was maintained at 5% by weight. In this regard, it is essential to understand different catalysts' performance for adsorption capacity and catalytic activity in ozone under various conditions [31]. Thus, 200 ppm of toluene was sent into the reactor with air at a total flow rate of 1000 lph. Adsorption was performed up to the breakthrough of toluene at the reactor outlet. The breakthrough curves of six catalysts and the corresponding toluene lost during the experiment are displayed in Figure 5. Once the toluene breakthrough was attained, the reactor was flushed with air to remove loosely bonded (physisorbed) toluene from the catalyst surface. A strongly or irreversibly bonded amount of toluene (chemisorbed) was obtained by subtracting the amount of toluene desorbed during flushing from the total amount of toluene adsorbed in the adsorption step.

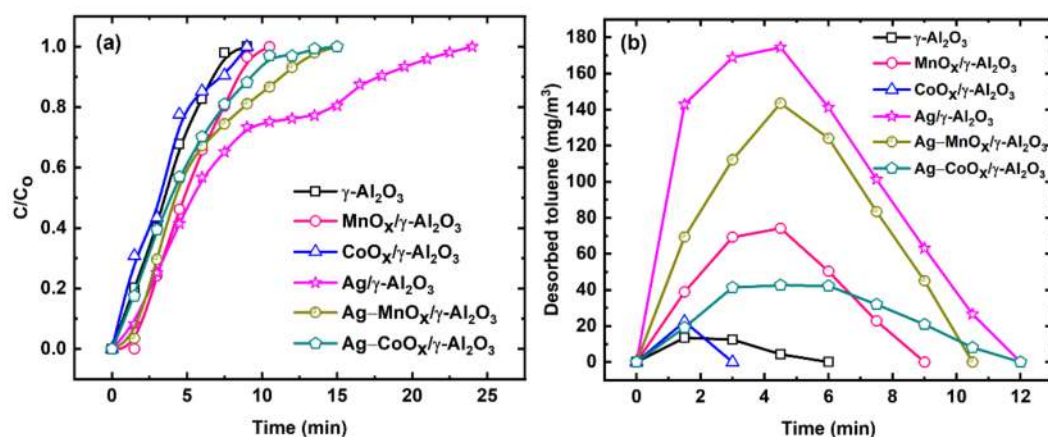


Figure 5. (a) Breakthrough curves of toluene; (b) amount of toluene desorbed as a function of time during ozone treatment of the catalysts.

In comparison to other catalysts, $\text{Ag}/\gamma\text{-Al}_2\text{O}_3$ has the longest breakthrough time, as shown in Figure 5a. It should be observed that metal oxide catalysts containing Ag had significantly greater toluene adsorption. Except for $\gamma\text{-Al}_2\text{O}_3$, all the catalysts had similar surface areas, implying that the increased toluene adsorption is not solely physical. The addition of Mn and Co alone does not have nearly the same impact as the addition of Ag. The number of active sites accessible for toluene adsorption increases because of Ag addition. Because of π -complexation, the d orbital of Ag^+ can bond with unsaturated hydrocarbons [31–33].

The chemisorbed toluene on the catalysts was desorbed using the strong oxidising agent ozone. The catalysts did not show any significant activity in removing toluene at room temperature. However, their activity was enhanced upon maintaining the desorption temperature at 75 °C. Furthermore, reports suggest that at temperatures higher than 80 °C, ozone decomposes and hence loses the ability to degrade the VOC [1,11]. Another reason can also be that there can be catalyst deactivation at room temperature due to the accumulation of carbonates on the surface of the catalysts. CO and CO_2 were the two main products of catalytic ozonation of toluene for the catalysts. Figure 6a,b show the amount of CO_2 and CO generated during the catalytic ozonation of the catalysts with respect to time. CO and CO_2 evolution peaked in the early stages of ozonation and then gradually declined. CO_x concentrations rise to a maximum before falling as the amount of toluene left on the catalyst diminishes as the reaction progresses. Among all the catalysts, $\text{Ag-CoO}_x/\gamma\text{-Al}_2\text{O}_3$ displayed the highest CO_2 concentration. The CO_2 evolution trend of the catalysts is as follows: $\text{Ag-CoO}_x/\gamma\text{-Al}_2\text{O}_3 > \text{Ag}/\gamma\text{-Al}_2\text{O}_3 > \text{Ag-MnO}_x/\gamma\text{-Al}_2\text{O}_3 > \text{MnO}_x/\gamma\text{-Al}_2\text{O}_3 > \text{CoO}_x/\gamma\text{-Al}_2\text{O}_3 \sim \gamma\text{-Al}_2\text{O}_3$.

Figure 6c,d show the CO_2 and CO selectivity of all the catalysts. Except for bare $\gamma\text{-Al}_2\text{O}_3$, the CO_2 selectivity decreased to a minimum before increasing and reaching a constant value. Kim et al. reported that the selectivity of CO_2 in gas-phase toluene decomposition is less than that of toluene adsorbed on the catalysts [34]. The trend in CO_2 selectivity may be attributed to the desorption of toluene during ozonation. Figure 7 shows that the amount of toluene desorbed during ozonation is less with $\text{Ag-CoO}_x/\gamma\text{-Al}_2\text{O}_3$, implying that a considerable portion of the adsorbed toluene undergoes oxidation rather than desorption. Figure 7 demonstrates the carbon balance of the synthesised catalysts after catalytic ozonation. $\text{Ag-CoO}_x/\gamma\text{-Al}_2\text{O}_3$ displayed the highest total carbon balance of 99.7%, of which 39.6% was lost during the flushing step while 52.4% was CO_x yield and 7.7% was recovered from toluene desorbed during ozonation.

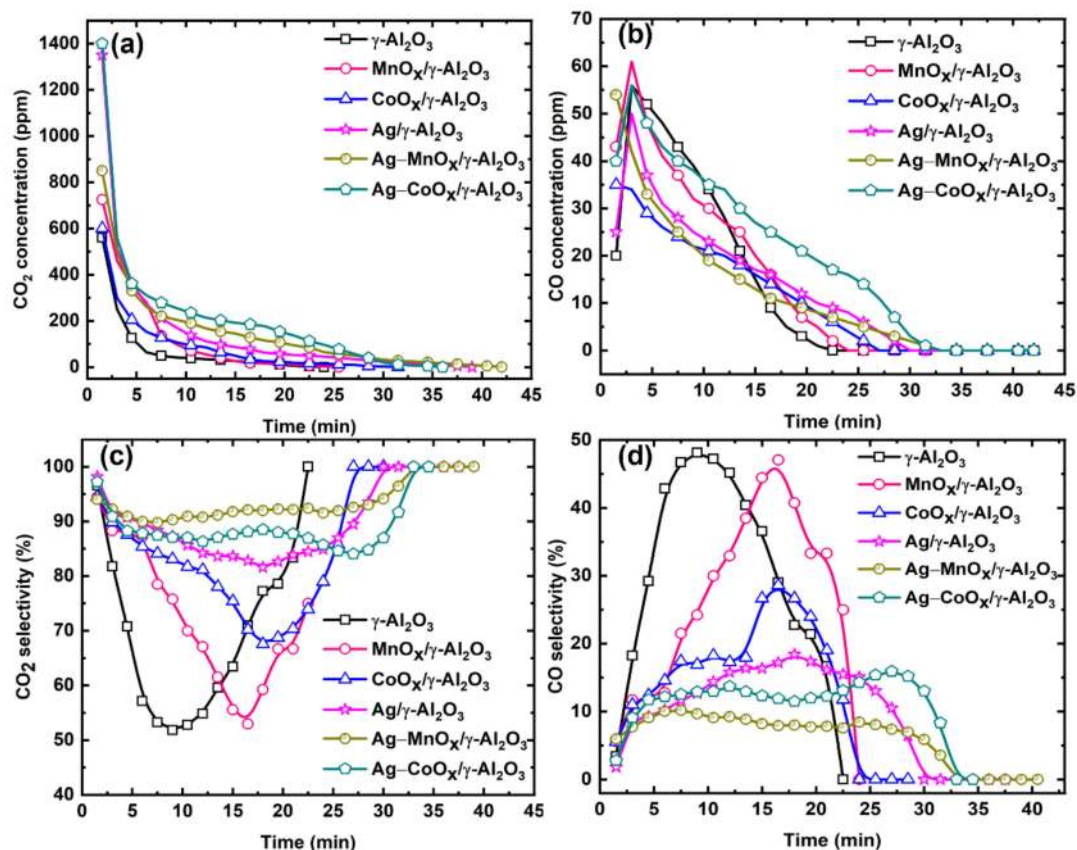


Figure 6. Variation of (a) CO₂, (b) CO, (c) CO₂ selectivity, and (d) CO selectivity with time obtained during ozone treatment.

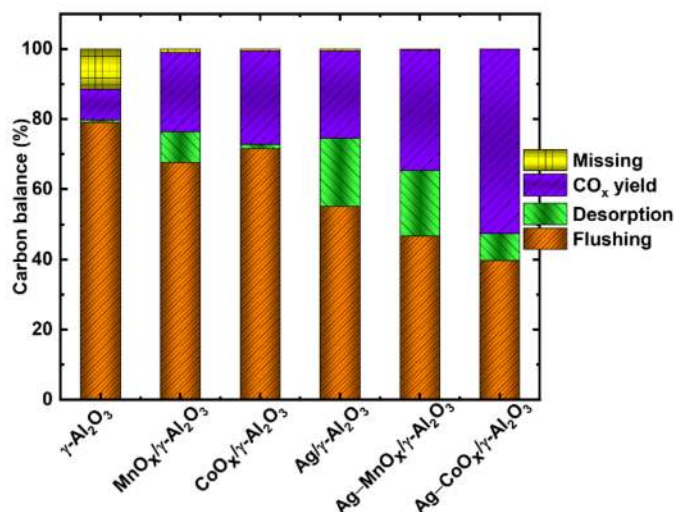


Figure 7. Carbon balance obtained during ozone treatment.

A comparison was made between Ag-impregnated metal oxides and pure metal oxides supported on γ -Al₂O₃. Metal oxides supported on γ -Al₂O₃ have higher activity than bare γ -Al₂O₃. However, toluene adsorption has been shown to impact active site mobility over Mn and Co based catalysts [35,36]. However, with the impregnation of Ag, the toluene adsorption increases due to the strong intermolecular force between Ag and toluene, thus creating the active site for reactions on the oxide surface [37]. In addition, the ratio of lattice oxygen to surface oxygen could be improved with Ag addition, boosting the catalytic

activity of Ag–CoO_x/γ-Al₂O₃ [38]. The presence of lattice oxygens in Ag–CoO_x/γ-Al₂O₃ facilitates the initial partial oxidation of toluene, which is then oxidised to CO and CO₂ due to the presence of O₃ [39].

Furthermore, literature studies show that the surface acidity of catalysts impacts catalytic activity for VOC degradation [39]. Because toluene adsorption occurs more readily on acidic surfaces, it may be harder to desorb it at low temperatures. The increased density of weakly acidic sites in Ag–CoO_x/γ-Al₂O₃ compared to other catalysts contributes to the catalyst's better activity. This quickly aids in surface adsorption and re-desorption of toluene at ambient temperature [40]. Table 3 provides a comparison between previous studies and the present work.

Table 3. A comparison of literature studies and the present study for catalytic ozonation of toluene.

Catalyst	Carrier Gas Flow Rate	Toluene Concentration	Ozone Concentration	Reaction Temperature (°C)	Toluene Removal Efficiency (%)	CO _x Selectivity (%)	Reference
Zeolite and MCM-41	0.12–0.39 m ³ /h	0.3–4.5 ppmv	0–80 ppmv	25 °C	96%	CO ₂ 95%	[41]
MnO ₂ -graphene	0.15 L/min	200 ppm	400 ppm	22 °C	33.6%		[42]
Pt or Pd-MnO _x /γ-Al ₂ O ₃	400 mL/min	120 ppm	1050 ppm	22–100 °C	100% (Pd) 85% (Pt)	90%	[1]
MnO _x /γ-Al ₂ O ₃ or SiO ₂ or TiO ₂	200 mL/min	100 ppm	1000 ppm	120 °C	>91%	>88%	[43]
Mn-M/HZSM-5 (M: Fe, Cu, Ru, Ag)	1 L/min	100 ppm	1000 ppm	25 °C	36% (RuMnZ)	~95%	[44]
Meso Mn/Al ₂ O ₃	1 L/min	50 ppm	1000 ppm	25 °C	100%	~80%	[26]
Pt-CeO ₂ /BEA	100 mL/min	35 ppm	350 ppm	25 °C	100%	70–100%	[45]
MnO _x on γ-Al ₂ O ₃ or MCM-41	400 mL/min	120 ppm	1050 ppm	22–100 °C	97% (80 °C)	93%	[10]
Ag-MO _x /γ-Al ₂ O ₃ (M = Mn/Co)	1000 L/h	200 ppm	500 ppm	75 °C		100%	Present work

3. Materials and Methods

3.1. Material Synthesis and Characterisation

Manganese and cobalt oxide supported on γ-Al₂O₃ were synthesised by the wet impregnation of γ-Al₂O₃ with the corresponding metal nitrate solution. Manganese (II) nitrate tetrahydrate, cobalt (II) nitrate hexahydrate and γ-Al₂O₃ (1/8-inch pellets) were obtained from Alfa Aesar (Haverhill, MA, USA). The γ-Al₂O₃ support was first calcined at 500 °C for four hours to remove the adsorbed impurities. The appropriate metal precursor solutions were added to γ-Al₂O₃ while stirring constantly and then dried overnight at 110 °C. Later, the dried samples were calcined at 500 °C for four hours in an air atmosphere. The precursor's amount was calculated such that the final metal loading was 5% by weight. Then, 2 wt% silver metal-supported manganese and cobalt oxides on γ-Al₂O₃ were prepared by depositing silver nitrate (Fisher Scientific, Waltham, MA, USA) on the synthesised MnO_x/γ-Al₂O₃ and CoO_x/γ-Al₂O₃ using a similar procedure. The obtained AgO_x-based catalysts were reduced by an H₂ flow of 30 mL/min at 200 °C for two hours.

Panalytical X'PERT PRO diffractometer (Malvern Panalytical Ltd, United Kingdom) with a CuK α radiation source (= 1.5418) was used to examine the catalysts' powder X-ray diffraction (XRD) patterns. Scans were collected in the range of 2θ between 10 and 90° with a scan rate of 0.01670° s⁻¹. The synthesised catalysts' specific surface area was determined using N₂ physisorption at –196 °C using Quantachrome, U.S.A., NOVA2200e surface area analyser (Boynton Beach, FL, United States). The surface area was measured between N₂ partial pressure ratio (P/P₀) of 0.05 to 0.3. Temperature-programmed desorption (TPD) tests were conducted using MicrotracBEL Corp. chemisorption apparatus (BEL Microtrac Co., Ltd., Tokyo, Japan) with a thermal conductivity detector. NH₃-TPD experiments were conducted to examine the acidic properties of the catalysts. After pre-treatment of the catalysts for one hour at 500 °C under He flow, they were cooled down to 100 °C, subsequently followed by adsorption of NH₃ from a flow of 5 vol.% NH₃/He at 100 °C. The flow was switched to pure He flow at the same temperature to remove any physisorbed

NH_3 . The TPD profile was then calculated by heating the samples linearly to $500\text{ }^\circ\text{C}$ at a rate of $10\text{ }^\circ\text{C min}^{-1}$ with a flow rate of 30 mL min^{-1} He. CO_2 -TPD experiments were conducted to investigate the basic nature of the catalysts. After pre-treatment of the catalysts for one hour at $300\text{ }^\circ\text{C}$ under He flow followed by cooling down to $100\text{ }^\circ\text{C}$, CO_2 adsorption was carried out in a flow of 10 vol.% CO_2/He at the same temperature. The flow was switched to pure He flow at the same temperature to remove any physisorbed CO_2 . Later, the TPD profile was recorded by heating the samples linearly to $900\text{ }^\circ\text{C}$ at $10\text{ }^\circ\text{C min}^{-1}$ under 30 mL min^{-1} He flow. The amount of NH_3/CO_2 desorbed from catalysts is represented by the area under the curve of the respective TPD profiles, which correlates to catalysts' acid/basic site density (mmol/g). The prepared catalysts' chemical state and surface composition were determined using X-ray photoelectron spectroscopy. Krato axis Ultra Spectrometer (Shimadzu Corp., Kyoto, Japan) with $\text{AlK}\alpha$ monochromatic excited radiation of 1489.5 eV with an emission current of 10 mA and applied voltage of 15 kV was used for the same procedure.

3.2. Experimental Setup

Catalytic activity was evaluated using a micro-fixed bed. Figure 8 depicts the experimental setup. A total of 10 g of the synthesised catalyst was filled between glass wool packing in a stainless-steel reactor with an internal diameter of 40 mm. The reactor was positioned inside an oven to control the reaction temperatures. Oxidation of toluene in the presence of ozone was used to determine the activity of the calcined catalysts. Before carrying out the reactions, the catalysts were not subjected to any pre-treatment and were used at room temperature and atmospheric pressure to mimic the industrial process. A toluene feed of 200 ppm was injected into the air stream (for balance) by a syringe pump (Ravel syringe infusion pump, RH-SY10 by Ravelhitek Pvt. Ltd., Chennai, Tamil Nadu). Airstream was supplied through a compressor at a rate of 1000 lph. Ozone was provided through a droplet ozone generator (output = 500 ppm of ozone per hour as analysed using Ozone monitor, API-450 Nema (Advanced Pollution Instrumentation, Inc., 2530 Patra Drive, El Sobrante, CA, USA)). Experiments were carried out in the following steps: The first step is the catalysts' saturation with toluene vapour until the toluene's outlet concentration matches the inlet concentration. After the breakthrough was achieved, the reactor was flushed with pure air (toluene feed was halted) to remove physisorbed toluene. Immediately, the oven temperature was increased to $75\text{ }^\circ\text{C}$ and ozone generator was turned on (airflow was discontinued) to measure the catalytic activity under different catalyst packing.

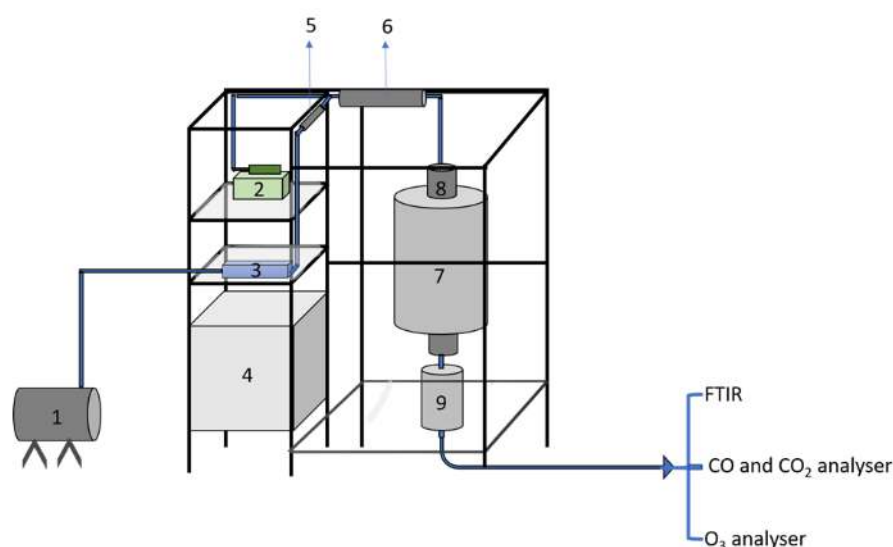


Figure 8. Experimental setup 1. Air compressor; 2. Syringe pump; 3. Rotameter; 4. Control unit; 5. Vaporiser; 6. Mixing chamber; 7. Heating coil (oven); 8. Stainless steel reactor; 9. Collector.

The toluene lost during flushing, CO_x yield obtained by the conversion of toluene to CO and CO₂, selectivity to CO₂, and the carbon balance were determined to assess the catalytic activity of the catalysts as given below:

$$\text{CO}_x \text{ yield}(\%) = \frac{n_{\text{CO}_2}^{\text{produced}} + n_{\text{CO}}^{\text{produced}}}{n_{\text{C}_7\text{H}_8}^{\text{adsorbed}} \times 7}$$

$$S_{\text{CO}_2}(\%) = \frac{\frac{C_{\text{CO}_2}}{44}}{\frac{C_{\text{CO}}}{28} + \frac{C_{\text{CO}_2}}{44}} \times 100$$

$$B_c(\%) = \frac{n_{\text{CO}_2}^{\text{produced}} + n_{\text{CO}}^{\text{produced}} + n_{\text{C}_7\text{H}_8}^{\text{flushed}} + n_{\text{C}_7\text{H}_8}^{\text{desorbed}} \times 7}{n_{\text{C}_7\text{H}_8}^{\text{adsorbed}} \times 7} \times 100$$

$$n_{\text{C}_7\text{H}_8}^{\text{adsorbed}} = \frac{\int_0^{t_a} F_a C_{(\text{C}_7\text{H}_8)_a} dt}{92}, n_{\text{C}_7\text{H}_8}^{\text{flushed}} = \frac{\int_0^{t_f} F_f C_{(\text{C}_7\text{H}_8)_a} dt}{92}, n_{\text{C}_7\text{H}_8}^{\text{desorbed}} = \frac{\int_0^{t_d} F_d C_{(\text{C}_7\text{H}_8)_d} dt}{92}$$

$$n_{\text{CO}}^{\text{produced}} = \frac{\int_0^{t_d} F_d C_{\text{CO}} dt}{28}, n_{\text{CO}_2}^{\text{produced}} = \frac{\int_0^{t_d} F_d C_{\text{CO}_2} dt}{44}$$

where $C_{(\text{C}_7\text{H}_8)_a}$ and $C_{(\text{C}_7\text{H}_8)_d}$ are the concentrations of toluene in the adsorption step and desorption step (mg m^{-3}). F_a , F_f and F_d are the flow rates of the airstream throughout the adsorption, flushing and desorption step. t_a , t_f and t_d are the adsorption time, flushing time, and desorption time (min). C_{CO} and C_{CO_2} are the concentrations of CO and CO₂ produced during the desorption step (mg m^{-3}). B_c is the carbon balance.

3.3. Analysis

A Fourier-transform infrared spectrometer (FTIR) (Bruker Tensor II, Billerica, MA, USA) equipped with a liquid N₂ cooled Mercury-Cadmium-Telluride detector and gas cell with a path length of 8 m was used to monitor toluene concentration near the outlet. Spectra were collected using OPUS software with 16 scans per spectrum and a spectral resolution of 0.5 cm^{-1} . Siemens Ultramat 23 (Siemens AG, Munich, Germany) was used to analyse CO_x products formed during ozonation.

4. Conclusions

Based on the catalytic ozonation of toluene using the synthesised catalysts, the toluene decomposition efficiencies varied with modifying the support surface with different transition metal oxides. The addition of Ag to the transition metal oxides significantly improved the activity of the catalyst. Ag–CoO_x/γ-Al₂O₃ had the highest ratio of surface acidic to basic sites, which improved toluene adsorption capacity on the catalyst. The formation of ample lattice oxygens and correspondingly having the highest $O_{\text{latt}}/O_{\text{surf}}$ ratio facilitated better toluene oxidation in the presence of the oxidising agent ozone. Hence, the CO_x selectivity and the carbon balance improved for Ag–CoO_x/γ-Al₂O₃.

Author Contributions: Conceptualisation, K.B., T.S. and C.S.; Formal analysis, K.B., D.R. and P.C.; Funding acquisition, T.S. and C.S.; Investigation, K.B., D.R. and P.C.; Methodology, K.B., D.R. and P.C.; Investigation, S.M.; Resources, S.M.; Project administration, C.S.; Supervision, C.S.; Writing—original draft, K.B.; Writing—review and editing, C.S. All authors have read and agreed to the published version of the manuscript.

Funding: The research was funded by DST-SERB (Project no.: E.M.R./2016/005636). The APC was self-funded.

Data Availability Statement: The data presented in this study are available on request from the corresponding author.

Acknowledgments: The author is immensely thankful to the DST-SERB (Project no.: E.M.R./2016/005636), India, for providing a junior research fellowship.

Conflicts of Interest: The authors declare no conflict of interest.

References

1. Rezaei, E.; Soltan, J.; Chen, N.; Lin, J. Effect of Noble Metals on Activity of $\text{MnO}_x/\gamma\text{-Alumina}$ Catalyst in Catalytic Ozonation of Toluene. *Chem. Eng. J.* **2013**, *214*, 219–228. [CrossRef]
2. An Indoor Air Purification Technology Using a Non-Thermal Plasma Reactor with Multiple-Wire-to-Wire Type Electrodes and a Fiber Air Filter—ScienceDirect. Available online: <https://www.sciencedirect.com/science/article/pii/S0304388616300717> (accessed on 22 December 2021).
3. Smith, J.F.; Gao, Z.; Zhang, J.S.; Guo, B. A New Experimental Method for the Determination of Emittable Initial VOC Concentrations in Building Materials and Sorption Isotherms for IVOCs. *CLEAN Soil Air Water* **2009**, *37*, 454–458. [CrossRef]
4. Mudliar, S.; Giri, B.; Padoley, K.; Satpute, D.; Dixit, R.; Bhatt, P.; Pandey, R.; Juwarkar, A.; Vaidya, A. Bioreactors for Treatment of VOCs and Odours—A Review. *J. Environ. Manag.* **2010**, *91*, 1039–1054. [CrossRef] [PubMed]
5. Hequet, V.; Raillard, C.; Debono, O.; Thévenet, F.; Locoge, N.; Coq, L.L. Photocatalytic Oxidation of VOCs at Ppb Level Using a Closed-Loop Reactor: The Mixture Effect. *Appl. Catal. B Environ.* **2018**, *226*, 473–486. [CrossRef]
6. Subrahmanyam, C.; Renken, A.; Kiwi-Minsker, L. Novel Catalytic Non-Thermal Plasma Reactor for the Abatement of VOCs. *Chem. Eng. J.* **2007**, *134*, 78–83. [CrossRef]
7. Karuppiah, J.; Reddy, E.L.; Reddy, P.M.K.; Ramaraju, B.; Karvembu, R.; Subrahmanyam, C. Abatement of Mixture of Volatile Organic Compounds (VOCs) in a Catalytic Non-Thermal Plasma Reactor. *J. Hazard. Mater.* **2012**, *237*, 283–289. [CrossRef]
8. Jia, Z.; Wang, X.; Thevenet, F.; Rousseau, A. Dynamic Probing of Plasma-Catalytic Surface Processes: Oxidation of Toluene on CeO_2 . *Plasma Process. Polym.* **2017**, *14*, 1600114. [CrossRef]
9. Yu, B.F.; Hu, Z.B.; Liu, M.; Yang, H.L.; Kong, Q.X.; Liu, Y.H. Review of Research on Air-Conditioning Systems and Indoor Air Quality Control for Human Health. *Int. J. Refrig.* **2009**, *32*, 3–20. [CrossRef]
10. Wang, S.; Ang, H.M.; Tade, M.O. Volatile Organic Compounds in Indoor Environment and Photocatalytic Oxidation: State of the Art. *Environ. Int.* **2007**, *33*, 694–705. [CrossRef]
11. Rezaei, E.; Soltan, J. Low Temperature Oxidation of Toluene by Ozone over $\text{MnO}_x/\gamma\text{-Alumina}$ and $\text{MnO}_x/\text{MCM-41}$ Catalysts. *Chem. Eng. J.* **2012**, *198*, 482–490. [CrossRef]
12. Wu, J.C.-S.; Lin, Z.-A.; Tsai, F.-M.; Pan, J.-W. Low-Temperature Complete Oxidation of BTX on Pt/Activated Carbon Catalysts. *Catal. Today* **2000**, *63*, 419–426. [CrossRef]
13. Huang, S.; Zhang, C.; He, H. Complete Oxidation of O-Xylene over Pd/ Al_2O_3 Catalyst at Low Temperature. *Catal. Today* **2008**, *139*, 15–23. [CrossRef]
14. Gervasini, A.; Vezzoli, G.C.; Ragaini, V. VOC Removal by Synergic Effect of Combustion Catalyst and Ozone. *Catal. Today* **1996**, *29*, 449–455. [CrossRef]
15. Liu, Y.; Zhou, H.; Cao, R.; Liu, X.; Zhang, P.; Zhan, J.; Liu, L. Facile and Green Synthetic Strategy of Birnessite-Type MnO_2 with High Efficiency for Airborne Benzene Removal at Low Temperatures. *Appl. Catal. B Environ.* **2019**, *245*, 569–582. [CrossRef]
16. Zhu, X.; Zhang, S.; Yu, X.; Zhu, X.; Zheng, C.; Gao, X.; Luo, Z.; Cen, K. Controllable Synthesis of Hierarchical $\text{MnO}_x/\text{TiO}_2$ Composite Nanofibers for Complete Oxidation of Low-Concentration Acetone. *J. Hazard. Mater.* **2017**, *337*, 105–114. [CrossRef]
17. Shi, F.; Wang, F.; Dai, H.; Dai, J.; Deng, J.; Liu, Y.; Bai, G.; Ji, K.; Au, C.T. Rod-, Flower-, and Dumbbell-like MnO_2 : Highly Active Catalysts for the Combustion of Toluene. *Appl. Catal. Gen.* **2012**, *433*, 206–213. [CrossRef]
18. Wang, F.; Dai, H.; Deng, J.; Bai, G.; Ji, K.; Liu, Y. Manganese Oxides with Rod-, Wire-, Tube-, and Flower-like Morphologies: Highly Effective Catalysts for the Removal of Toluene. *Environ. Sci. Technol.* **2012**, *46*, 4034–4041. [CrossRef]
19. Zhao, D.-Z.; Shi, C.; Li, X.-S.; Zhu, A.-M.; Jang, B.W.-L. Enhanced Effect of Water Vapor on Complete Oxidation of Formaldehyde in Air with Ozone over MnO_x Catalysts at Room Temperature. *J. Hazard. Mater.* **2012**, *239*, 362–369. [CrossRef]
20. Lin, F.; Zhang, Z.; Xiang, L.; Zhang, L.; Cheng, Z.; Wang, Z.; Yan, B.; Chen, G. Efficient Degradation of Multiple Cl-VOCs by Catalytic Ozonation over MnO_x Catalysts with Different Supports. *Chem. Eng. J.* **2022**, *435*, 134807. [CrossRef]
21. Tian, M.; Liu, S.; Wang, L.; Ding, H.; Zhao, D.; Wang, Y.; Cui, J.; Fu, J.; Shang, J.; Li, G.K. Complete Degradation of Gaseous Methanol over Pt/ FeO_x Catalysts by Normal Temperature Catalytic Ozonation. *Environ. Sci. Technol.* **2020**, *54*, 1938–1945. [CrossRef]
22. He, C.; Liao, Y.; Chen, C.; Xia, D.; Wang, Y.; Tian, S.; Yang, J.; Shu, D. Realising a Redox-Robust Ag/ MnO_2 Catalyst for Efficient Wet Catalytic Ozonation of S-VOCs: Promotional Role of Ag(0)/Ag(I)-Mn Based Redox Shuttle. *Appl. Catal. B Environ.* **2022**, *303*, 120881. [CrossRef]
23. Subrahmanyam, C.; Magureanu, M.; Renken, A.; Kiwi-Minsker, L. Catalytic Abatement of Volatile Organic Compounds Assisted by Non-Thermal Plasma: Part 1. A Novel Dielectric Barrier Discharge Reactor Containing Catalytic Electrode. *Appl. Catal. B Environ.* **2006**, *65*, 150–156. [CrossRef]
24. Subrahmanyam, C.; Renken, A.; Kiwi-Minsker, L. Catalytic Abatement of Volatile Organic Compounds Assisted by Non-Thermal Plasma: Part II. Optimized Catalytic Electrode and Operating Conditions. *Appl. Catal. B Environ.* **2006**, *65*, 157–162. [CrossRef]
25. Cao, F.; Xiang, J.; Su, S.; Wang, P.; Hu, S.; Sun, L. Ag Modified Mn-Ce/ $\gamma\text{-Al}_2\text{O}_3$ Catalyst for Selective Catalytic Reduction of NO with NH_3 at Low-Temperature. *Fuel Process. Technol.* **2015**, *135*, 66–72. [CrossRef]
26. Ryu, H.W.; Song, M.Y.; Park, J.S.; Kim, J.M.; Jung, S.-C.; Song, J.; Kim, B.-J.; Park, Y.-K. Removal of Toluene Using Ozone at Room Temperature over Mesoporous Mn/ Al_2O_3 Catalysts. *Environ. Res.* **2019**, *172*, 649–657. [CrossRef]

27. Aboelazm, E.A.; Ali, G.A.; Chong, K.F. Cobalt Oxide Supercapacitor Electrode Recovered from Spent Lithium-Ion Battery. *Chem. Adv. Mater.* **2018**, *3*, 67–73.
28. Zhan, S.; Hou, Q.; Li, Y.; Ma, S.; Wang, P.; Li, Y.; Wang, H. AgBr/g-C₃N₄ Nanocomposites for Enhanced Visible-Light-Driven Photocatalytic Inactivation of *Escherichia Coli*. *RSC Adv.* **2018**, *8*, 34428–34436. [[CrossRef](#)]
29. Qu, Z.; Bu, Y.; Qin, Y.; Wang, Y.; Fu, Q. The Improved Reactivity of Manganese Catalysts by Ag in Catalytic Oxidation of Toluene. *Appl. Catal. B Environ.* **2013**, *132*, 353–362. [[CrossRef](#)]
30. Chawdhury, P.; Kumar, D.; Subrahmanyam, C. NTP Reactor for a Single Stage Methane Conversion to Methanol: Influence of Catalyst Addition and Effect of Promoters. *Chem. Eng. J.* **2019**, *372*, 638–647. [[CrossRef](#)]
31. Xu, X.; Wang, P.; Xu, W.; Wu, J.; Chen, L.; Fu, M.; Ye, D. Plasma-Catalysis of Metal Loaded SBA-15 for Toluene Removal: Comparison of Continuously Introduced and Adsorption-Discharge Plasma System. *Chem. Eng. J.* **2016**, *283*, 276–284. [[CrossRef](#)]
32. Nguyen, V.T.; Nguyen, D.B.; Mok, Y.S.; Hossain, M.D.M.; Saud, S.; Yoon, K.H.; Dinh, D.K.; Ryu, S.; Jeon, H.; Kim, S.B. Removal of Ethyl Acetate in Air by Using Different Types of Corona Discharges Generated in a Honeycomb Monolith Structure Coated with Pd/ γ -Alumina. *J. Hazard. Mater.* **2021**, *416*, 126162. [[CrossRef](#)] [[PubMed](#)]
33. Trinh, Q.H.; Lee, S.B.; Mok, Y.S. Removal of Ethylene from Air Stream by Adsorption and Plasma-Catalytic Oxidation Using Silver-Based Bimetallic Catalysts Supported on Zeolite. *J. Hazard. Mater.* **2015**, *285*, 525–534. [[CrossRef](#)] [[PubMed](#)]
34. Kim, H.-H.; Sugawara, M.; Hirata, H.; Teramoto, Y.; Kosuge, K.; Negishi, N.; Ogata, A. Ozone-Assisted Catalysis of Toluene with Layered ZSM-5 and Ag/ZSM-5 Zeolites. *Plasma Chem. Plasma Process.* **2013**, *33*, 1083–1098. [[CrossRef](#)]
35. Wang, W.; Wang, H.; Zhu, T.; Fan, X. Removal of Gas Phase Low-Concentration Toluene over Mn, Ag and Ce Modified HZSM-5 Catalysts by Periodical Operation of Adsorption and Non-Thermal Plasma Regeneration. *J. Hazard. Mater.* **2015**, *292*, 70–78. [[CrossRef](#)]
36. Santos, V.P.; Pereira, M.F.R.; Órfão, J.J.M.; Figueiredo, J.L. The Role of Lattice Oxygen on the Activity of Manganese Oxides towards the Oxidation of Volatile Organic Compounds. *Appl. Catal. B Environ.* **2010**, *99*, 353–363. [[CrossRef](#)]
37. Tang, C.; Huang, X.; Wang, H.; Shi, H.; Zhao, G. Mechanism Investigation on the Enhanced Photocatalytic Oxidation of Nonylphenol on Hydrophobic TiO₂ Nanotubes. *J. Hazard. Mater.* **2020**, *382*, 121017. [[CrossRef](#)]
38. Cellier, C.; Lambert, S.; Gaigneaux, E.M.; Poleunis, C.; Ruaux, V.; Eloy, P.; Lahousse, C.; Bertrand, P.; Pirard, J.-P.; Grange, P. Investigation of the Preparation and Activity of Gold Catalysts in the Total Oxidation of N-Hexane. *Appl. Catal. B Environ.* **2007**, *70*, 406–416. [[CrossRef](#)]
39. Li, J.; Na, H.; Zeng, X.; Zhu, T.; Liu, Z. In Situ DRIFTS Investigation for the Oxidation of Toluene by Ozone over Mn/HZSM-5, Ag/HZSM-5 and Mn–Ag/HZSM-5 Catalysts. *Appl. Surf. Sci.* **2014**, *311*, 690–696. [[CrossRef](#)]
40. Kim, J.; Kwon, E.E.; Lee, J.E.; Jang, S.-H.; Jeon, J.-K.; Song, J.; Park, Y.-K. Effect of Zeolite Acidity and Structure on Ozone Oxidation of Toluene Using Ru–Mn Loaded Zeolites at Ambient Temperature. *J. Hazard. Mater.* **2021**, *403*, 123934. [[CrossRef](#)]
41. Kwong, C.W.; Chao, C.Y.H.; Hui, K.S.; Wan, M.P. Catalytic Ozonation of Toluene Using Zeolite and MCM-41 Materials. *Environ. Sci. Technol.* **2008**, *42*, 8504–8509. [[CrossRef](#)]
42. Hu, M.; Hui, K.S.; Hui, K.N. Role of Graphene in MnO₂/Graphene Composite for Catalytic Ozonation of Gaseous Toluene. *Chem. Eng. J.* **2014**, *254*, 237–244. [[CrossRef](#)]
43. Low Temperature Catalytic Ozonation of Toluene in Flue Gas over Mn-Based Catalysts. Effect of Support Property and SO₂/Water Vapor Addition. *Elsevier Enhanced Reader*. Available online: <https://reader.elsevier.com/reader/sd/pii/S0926337320300771?token=CCC7B4C2A0090FF120B6E976AFE70D190814687F23BD668481936900E86751CBF86D851EC6D570AD826CE58BC83A567A&originRegion=eu-west-1&originCreation=20220217043031> (accessed on 17 February 2022).
44. Catalytic Ozonation of Toluene Using Mn–M Bimetallic HZSM-5 (M = Fe, Cu, Ru, Ag) Catalysts at Room Temperature. *Elsevier Enhanced Reader*. Available online: <https://reader.elsevier.com/reader/sd/pii/S0304389420305665?token=FB6B5FE8CD283B334B8F849012C9F79A68DA27C0DC05C8538F8E6AA73A2B93932311000B57F9496A9C81355F6DA12429&originRegion=eu-west-1&originCreation=20220217043205> (accessed on 17 February 2022).
45. Wang, J.; Shi, X.; Chen, L.; Li, H.; Mao, M.; Zhang, G.; Yi, H.; Fu, M.; Ye, D.; Wu, J. Enhanced Performance of Low Pt Loading Amount on Pt–CeO₂ Catalysts Prepared by Adsorption Method for Catalytic Ozonation of Toluene. *Appl. Catal. Gen.* **2021**, *625*, 118342. [[CrossRef](#)]